Convection induced by thermal gradients on thin reaction fronts

David R. A. Ruelas Paredes[1] and Desiderio A. Vasquez[1,2]

[1]*Departamento de Ciencias, Sección Física, Pontificia Universidad Católica del Perú Av. Universitaria 1801, San Miguel, Lima 32, Peru*

[2]*Department of Physics, Indiana University Purdue University Fort Wayne, Fort Wayne, Indiana 46805, USA*

(Received 27 June 2017; published 29 September 2017)

We present a thin front model for the propagation of chemical reaction fronts in liquids inside a Hele-Shaw cell or porous media. In this model we take into account density gradients due to thermal and compositional changes across a thin interface. The front separating reacted from unreacted fluids evolves following an eikonal relation between the normal speed and the curvature. We carry out a linear stability analysis of convectionless flat fronts confined in a two-dimensional rectangular domain. We find that all fronts are stable to perturbations of short wavelength, but they become unstable for some wavelengths depending on the values of compositional and thermal gradients. If the effects of these gradients oppose each other, we observe a range of wavelengths that make the flat front unstable. Numerical solutions of the nonlinear model show curved fronts of steady shape with convection propagating faster than flat fronts. Exothermic fronts increase the temperature of the fluid as they propagate through the domain. This increment in temperature decreases with increasing speed.

DOI: 10.1103/PhysRevE.96.033116

I. INTRODUCTION

Convective fluid motion arises from buoyancy forces due to density gradients. These density gradients can be due to changes in fluid composition, such as those present in Rayleigh-Taylor instabilities [1]. They can also be caused by thermal expansion, as is the case of the Rayleigh-Bénard instability [2], when a fluid is heated from below. We find both types of mechanisms in chemical reaction fronts propagating in liquids. These systems consist of an interface separating fluids of different composition, thus allowing the possibility of a Rayleigh-Taylor instability. At the same time, the chemical reaction can release heat, resulting in a hydrodynamic instability caused by thermal expansion. Examples of these fronts can be found in combustion where chemical reactions are exothermic [3]. Compositional and thermal gradients lead to convection in polymerization fronts [4], and also in autocatalytic chemical reactions propagating in liquids such as the iron(II)-nitric acid reaction [5], the iodate-sulfite reaction [6], the chlorite-tetrathionate reaction [7–9], and the iodate-arsenous acid (IAA) reaction [10].

Previous theoretical work described the front propagation in liquids using reaction-diffusion-convection equations coupled to the appropriate hydrodynamics and the heat equation. Different chemical reactions required different reaction terms: a cubic polynomial for the IAA reaction [11–13] and a fourth-order polynomial for a model of the chlorite-tetrathionate reaction [14,15]. In these works, fluid density was considered a linear function of temperature and chemical concentration. These theories were also applied to three-dimensional convective systems with thermal and compositional gradients [9,16].

The propagation of the reaction fronts can also be modeled using a thin interface separating the reactants from the products. In this case, the normal speed of the front is determined by the local front curvature using an eikonal relation. The results for the linear stability analysis of flat fronts in the IAA reaction using the eikonal relation are close to the results using a reaction-diffusion model [17]. For this reaction, the eikonal relation showed good agreement with the speeds of convective fronts in vertical cylinders [18,19]. The heat effects in the stability of the flat fronts were also described with the same approach [20]. The results of the thin front model can be applied to other reactions since it depends only on the front curvature with the chemical reaction taking place in the very thin interface.

In this paper, we study the effects of thermal expansion using a thin front model. The heat release takes place only at the interface separating reacted from unreacted fluids. We include thermal and compositional gradients to analyze the stability of an unbounded horizontal flat front. We also investigate the change in shape and increase of speed for fronts propagating in vertical domains near the onset of convection.

II. THEORETICAL FRAMEWORK

A. Equations of motion

We study autocatalytic reaction fronts propagating upward in aqueous solutions. The front separates reacted from unreacted fluids leading to density gradients across the front. We consider fluids confined inside a Hele-Shaw cell or a two-dimensional porous media; therefore, their velocities obey Darcy's law:

$$\mathbf{v}(x,y,t) = -\frac{\kappa}{\mu}(\nabla P + \rho \mathbf{g}). \tag{1}$$

Here κ is the permeability of the medium, μ is the dynamic viscosity of the fluid, P is the pressure, ρ is the fluid density, and $\mathbf{g}$ is the acceleration of gravity. We work in a laboratory reference frame where the x axis is horizontal and gravity points in the negative y direction: $\mathbf{g} = -g\hat{y}$. The fluid velocity also satisfies a mass continuity equation, which in the Boussinesq approximation [21] becomes

$$\nabla \cdot \mathbf{v} = 0. \tag{2}$$

This equation allows us to replace the fluid velocity field with a stream function $\psi(x,y,t)$, having the fluid velocity components as $v_x = -\partial\psi/\partial y$ and $v_y = \partial\psi/\partial x$. We can eliminate the pressure by taking the curl of Eq. (1) leading

to a Poisson equation for the stream function:

$$\nabla^2\psi = -\frac{\kappa g}{\mu}\frac{\partial \rho}{\partial x}. \tag{3}$$

We model the reaction front as a thin interface located by a height function $H(x,t)$. An eikonal relation between the flat front velocity and the curvature of the front provides the normal front velocity thus resulting in a rule to propagate the front. For fronts propagating in moving fluids, we add the normal fluid velocity to the eikonal relation. For small curvatures and slow fluid speeds the eikonal relation leads to

$$\frac{\partial H}{\partial t} = C_0 + \frac{C_0}{2}\left(\frac{\partial H}{\partial x}\right)^2 + D_C\frac{\partial^2 H}{\partial x^2} + v_y|_{y=H}, \tag{4}$$

where C_0 is the flat front speed and D_C the fluid molecular diffusivity [22]. This equation corresponds to a deterministic Kardar-Zhang-Parisi equation coupled to fluid flow.

To account for thermal effects we include a heat equation advected by the fluid velocity with a front-centered delta function as a heat source. The equation for the temperature of the fluid $T(x,y,t)$ corresponds to

$$\frac{\partial T}{\partial t} + \mathbf{v}\cdot\boldsymbol{\nabla} T = D_T\nabla^2 T + Q\delta(y-H). \tag{5}$$

Here D_T represents the thermal diffusivity, and the constant Q sets the amount of heat released at the front position. We do not include slope corrections for the delta function since our focus is on fronts near the onset of convection. We assume that the fluid density varies linearly with T having a discontinuous jump due to the change in composition at the front:

$$\rho(x,y,t) = \rho_0[1-\alpha(T-T_0)+\beta\Theta(y-H)]. \tag{6}$$

Here ρ_0 is the density of the unreacted fluid at temperature T_0, α the thermal expansion coefficient, β the fractional change in density across the front, and $\Theta(y-H)$ the Heaviside step function. The boundary conditions correspond to no diffusive flow across the wall, which leads to $\partial H/\partial x = 0$ for the front height. There is no heat flow through the walls, therefore, the normal derivatives of T at the bottom and lateral walls are zero. Ahead and far away from the front the temperature is set to T_0.

A convectionless solution of Eqs. (3)–(5) travels upward with constant speed C_0 having a temperature profile equal to

$$T^{(0)} = \begin{cases} T_0 + Q/C_0, & \text{for } y < 0, \\ T_0 + (Q/C_0)e^{-C_0 y/D_T}, & \text{for } y \geqslant 0. \end{cases} \tag{7}$$

This steady state temperature solution corresponds to a reference frame moving along the vertical y coordinate with constant velocity C_0. The front position is located at $H^{(0)} = 0$, with the stream function equal to $\psi^{(0)} = 0$ representing zero velocity in the laboratory frame. The zero superindex labels this particular solution which has a constant temperature below the front decreasing exponentially toward the unreacted fluid temperature T_0. Far below the front the temperature of the reacted fluid corresponds to $T_1 \equiv T_0 + \Delta T$, with $\Delta T = Q/C_0$.

We introduce dimensionless units using $\tau \equiv D_T C_0^{-2}$ for time and $\ell \equiv D_T C_0^{-1}$ for length. With these definitions we have the dimensionless coordinates and variables given by $x = x'\ell$, $t = t'\tau$, $H = H'\ell$, $T = T'\Delta T$, and $\psi = \psi'\ell^2\tau^{-1}$. After dropping the primes, we are left with the following nonlinear system:

$$\frac{\partial T}{\partial t} = \nabla^2 T - \mathbf{v}\cdot\boldsymbol{\nabla} T + \delta(y-H) + \frac{\partial T}{\partial y}, \tag{8a}$$

$$\nabla^2\psi = \mathrm{Ra_T}\frac{\partial T}{\partial x} + \mathrm{Ra_C}\frac{\partial H}{\partial x}\delta(y-H), \tag{8b}$$

$$\frac{\partial H}{\partial t} = \frac{1}{2}\left(\frac{\partial H}{\partial x}\right)^2 + \frac{1}{\mathscr{L}}\frac{\partial^2 H}{\partial x^2} + v_y|_{y=H}. \tag{8c}$$

The last term in Eq. (8a) arises from using a comoving reference frame; the first term in Eq. (4) vanishes for the same reason. The system is defined by three dimensionless numbers: $\mathrm{Ra_T}$, $\mathrm{Ra_C}$, and $\mathscr{L}$. The first two are, respectively, the thermal and compositional Rayleigh numbers:

$$\mathrm{Ra_T} \equiv \frac{\kappa g\rho_0\alpha\Delta T}{\mu C_0}, \quad \mathrm{Ra_C} \equiv \frac{\kappa g\rho_0\beta}{\mu C_0}. \tag{9}$$

The Lewis number $\mathscr{L}$ is the ratio between thermal and molecular diffusivities, $\mathscr{L} \equiv D_T/D_C$. In this paper we will use values related to experiments in the iodate-arsenous acid reaction where the thermal diffusivity is [23] $D_T = 1.45\times10^{-3}$ cm^2/s and the molecular diffusivity is $D_C = 2\times10^{-5}$ cm^2/s, resulting in a Lewis number $\mathscr{L} = 72.5$.

B. Linear stability analysis

We carry out a linear stability analysis to determine the stability of the flat front solutions with respect to small perturbations. A new variable for the temperature is introduced by defining $T = T^{(0)} + T^{(1)}$, with $T^{(1)}$ being a perturbation to the convectionless solution. Similarly, we introduce perturbations to the front height and the stream function. Substituting the variables into Eq. (8a), it reads

$$\frac{\partial T^{(1)}}{\partial t} + \mathbf{v^{(1)}}\cdot\boldsymbol{\nabla}(T^{(0)}+T^{(1)}) = \frac{d^2T^{(0)}}{dy^2} + \nabla^2 T^{(1)} + \delta(y-H^{(1)}) + \frac{dT^{(0)}}{dy} + \frac{\partial T^{(1)}}{\partial y}. \tag{10}$$

A Taylor series expansion helps to evaluate the delta function for small front heights: $\delta(x-H^{(1)}) \approx \delta(x) - H^{(1)}\delta'(x)$. Neglecting second order terms, together with the fact that $T^{(0)}$ is a solution for the convectionless front, we arrive at a set of linear equations describing the evolution of the perturbations,

$$\frac{\partial T^{(1)}}{\partial t} + \mathbf{v^{(1)}}\cdot\boldsymbol{\nabla} T^{(0)} = \nabla^2 T^{(1)} - H^{(1)}\delta'(x) + C_0\frac{\partial T^{(1)}}{\partial x}, \tag{11a}$$

$$\nabla^2\psi^{(1)} = \mathrm{Ra_T}\frac{\partial T^{(1)}}{\partial y} + \mathrm{Ra_C}\frac{\partial H^{(1)}}{\partial y}\delta(x), \tag{11b}$$

$$\frac{\partial H^{(1)}}{\partial t} = \frac{1}{\mathscr{L}}\frac{\partial^2 H^{(1)}}{\partial y^2} + {v_x}^{(1)}. \tag{11c}$$

Since Eqs. (11) are linear, we can introduce plane waves that extend along the horizontal direction having wave number

q. Taking into account the boundary conditions, we write the perturbations as

$$T^{(1)} = T_q(y,t)\cos(qx), \tag{12a}$$

$$\psi^{(1)} = \psi_q(y,t)\sin(qx), \tag{12b}$$

$$H^{(1)} = H_q(y,t)\cos(qx). \tag{12c}$$

After substituting Eqs. (12) into Eqs. (11) and simplifying, we obtain a system for the time evolution of the plane wave perturbations:

$$\frac{\partial T_q}{\partial t} = \frac{\partial^2 T_q}{\partial y^2} - q^2 T_q - q\psi_q \frac{dT^{(0)}}{dy} - H_q\delta'(y) + \frac{\partial T_q}{\partial y}, \tag{13a}$$

$$\frac{\partial^2 \psi_q}{\partial y^2} = q^2\psi_q - q\,\mathrm{Ra_T} T_q - q\,\mathrm{Ra_C} H_q\delta(y), \tag{13b}$$

$$\frac{\partial H_q}{\partial t} = -\frac{q^2}{\mathscr{L}} H_q + q\psi_q|_{y=0}. \tag{13c}$$

Since these equations vary linearly with time, we look for solutions where the variables of temperature, height, and stream function are proportional to $e^{\sigma t}$. The stability of the flat front solution is determined by the sign of the growth rate σ for a given value of the wave number q, if σ is positive then the perturbations will grow indefinitely with the front being unstable. If the growth rate is negative, the flat front is stable since the perturbations will vanish after a long time.

III. NUMERICAL METHODS

We solve the linear and nonlinear partial differential equations using numerical techniques. A rectangular mesh is set to approximate all spatial derivatives using second order finite difference schemes. The time evolution is carried out by using a first order finite difference approximation allowing one to calculate the temperature and height variables after a small time step [24]. The stream function is calculated by solving the discretized Poisson equation (8b) using an alternating-direction relaxation method [25]. Our results were compared with the solution of the Poisson equation using the GENBUN subroutine of the FISHPACK package [26] finding good agreement between both methods.

Our equations involve Dirac's δ function and its derivative, δ'. We approximate both with representations in terms of a small parameter, ϵ. For the δ functions we use the Poisson kernel,

$$\delta_\epsilon(y-H) = \frac{1}{\pi}\frac{\epsilon}{(y-H)^2+\epsilon^2}, \tag{14}$$

which equals $\delta(y-H)$ in the limit $\epsilon \to 0$. To implement δ' we opt for a "rectangular" representation [27]:

$$\delta'_\epsilon(y) = \begin{cases} 0, & \text{if } y < -\epsilon, \\ -1/\epsilon^2, & \text{if } -\epsilon < y < 0, \\ 1/\epsilon^2, & \text{if } 0 < y < \epsilon, \\ 0, & \text{if } y > \epsilon. \end{cases} \tag{15}$$

The value of ϵ is comparable to the distance between adjacent grid points. We set the mesh size $\Delta y = 0.1875$ and time step $\Delta t = 10^{-3}$ for the linear calculations. To solve the nonlinear Poisson equation with GENBUN, we work on a two-dimensional grid with $\Delta x = 4.54 \times 10^{-2}$ and $\Delta y = 6.25 \times 10^{-2}$; the corresponding time step is $\Delta t = 5 \times 10^{-4}$. When working with the alternating-directions implicit method we use a range of mesh sizes and time steps close to the previous values.

Studying the time evolution of small random perturbations on the plane wave expansion [Eq. (13c)] allows us to calculate their growth rate. After a long time, the system variables evolve proportional to $e^{\sigma(q)t}$; therefore, σ can be obtained from the time evolution. If $\sigma(q)$ is positive, the perturbations will grow indefinitely eventually reaching extremely large numbers. To avoid this problem, after a certain time, all the variables are multiplied by a normalizing factor, with the new variables evolving with the same exponential rate. A similar approach is used when $\sigma(q)$ is negative as the numbers will eventually become too small. Since the front travels upward, the singularity of $\delta(y-H)$ shifts with time. We switch to a system that moves with the speed of the average front position allowing us to keep the system variables within our computational domain.

IV. RESULTS

A. Linear stability analysis results

To study the importance of thermal expansion, we carry out a linear stability analysis of convectionless flat fronts without compositional gradients ($\mathrm{Ra_C} = 0$). The resulting dispersion relations in Fig. 1 show the dependence of the growth rate σ with respect to the corresponding wave number q for different values of the thermal Rayleigh number $\mathrm{Ra_T}$. Here we focus on exothermic reactions where $\mathrm{Ra_T}$ is positive, which results in having the less dense fluid underneath heavier cold fluid. In all of these cases we find dispersion relations having a maximum growth rate that is positive, indicating that the front is unstable for perturbations of certain wave number. For zero wave numbers, the growth rate is zero; however, the slope

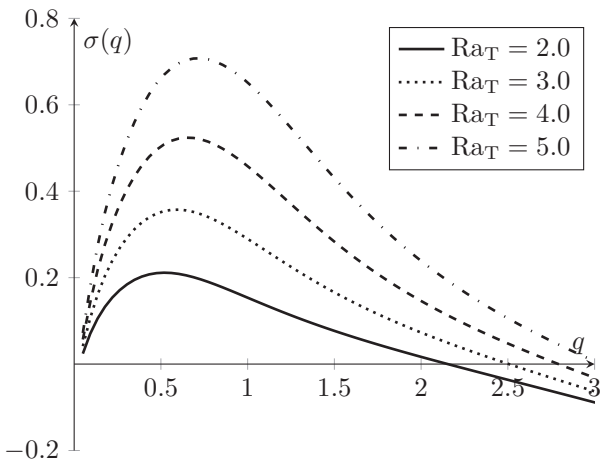

FIG. 1. Dispersion curves for different values of $\mathrm{Ra_T}$, with $\mathrm{Ra_C} = 0$. Unstable perturbations correspond to wave numbers with positive values of sigma. The range of wave numbers leading to instabilities increases as $\mathrm{Ra_T}$ is increased.

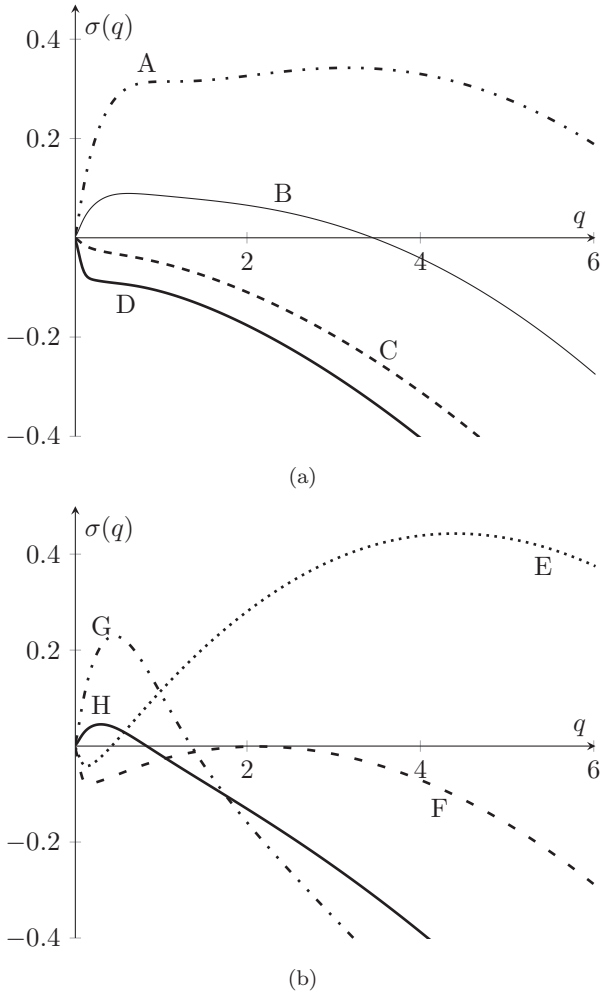

FIG. 2. Dispersion relations for compositional and thermal Rayleigh numbers of (a) the same sign and (b) opposite signs. In (a), curve A corresponds to $Ra_C = 0.3$ and $Ra_T = 2$, curve B to $Ra_C = 0.1$ and $Ra_T = 0.75$, curve C to $Ra_C = -0.05$ and $Ra_T = -0.25$, and curve D to $Ra_C = -0.1$ and $Ra_T = -1.5$. In (b), curve E corresponds to $Ra_C = 0.4$ and $Ra_T = -1.5$, curve F to $Ra_C = 0.1$ and $Ra_T = -2$, curve G to $Ra_C = -0.2$ and $Ra_T = 2.5$, and curve H to $Ra_C = -0.1$ and $Ra_T = 0.75$.

of the dispersion relation is positive; thus perturbations with nonzero but small wave numbers (large wavelengths) will have a destabilizing effect. Since the growth rate is negative for very large wave numbers there is a critical wave number where the growth rate is exactly zero. This fact shows that flat fronts propagating in narrow tubes are stable since the tube width only allows perturbations of small wavelengths which have negative growth rate. We notice that for higher values of Ra_T the range of wave numbers that have positive growth rate increases, with the maximum growth rate becoming larger; consequently the flat front becomes more unstable. As long as the front propagates in a wide enough tube, the exothermicity of the reaction will always make the flat front unstable.

In the presence of compositional gradients, thermal gradients will affect the front stability depending on the combined effects of both gradients on the density. In the case of having both Rayleigh numbers positive, we find that perturbations of small wave numbers will always have positive growth rate, indicating an unstable flat front. We show in Fig. 2(a) dispersion relations for two sets of positive Rayleigh numbers. The dispersion relation corresponding to $Ra_T = 2.0$ and $Ra_C = 0.3$ has higher growth rates compared to the one with $Ra_T = 0.75$ and $Ra_C = 0.1$; this is due to the fact that each respective Rayleigh number is higher. In the case where both Rayleigh numbers are negative, we find negative growth rates for all perturbations; therefore, the flat front is stable. The stronger the Rayleigh numbers in the negative direction the more negative the values of the growth rate as displayed in lines C and D of Fig. 2(a); therefore, favorable density gradients enhance the stability of the flat front.

When the compositional and thermal Rayleigh numbers have opposite signs the onset of convection will depend on their relative strength. In the case of having a negative Ra_T, we find that small values of Ra_C could lead to an unstable flat front. In curve F of Fig. 2(b) we show a case where the growth rates are negative, but the curve exhibits a relative maximum very close to zero. Slightly increasing the compositional Rayleigh number will result in having some growth rates positive. Here the onset of the instability takes place at a wave number away from zero, in contrast to having both Rayleigh numbers positive, where wave numbers close to zero always have positive growth rates. Away from the critical case, we find a range of wave numbers with positive growth rates, as shown in curve E. This result was also found in a hydrodynamic reaction-diffusion model for the chlorite-tetrathionate reaction [14]. Here wave numbers close to zero have negative growth rates, as well as large wave numbers. In the case of having a positive Ra_T, we find that wave numbers near zero show positive growth rates, thus allowing instabilities at large wavelengths as shown in curves G and H of Fig. 2(b).

The stability of the flat front as a function of the compositional and thermal Rayleigh numbers is shown in Fig. 3. In this figure we indicate two different regions in the Ra_C-Ra_T plane where combinations of these Rayleigh numbers results

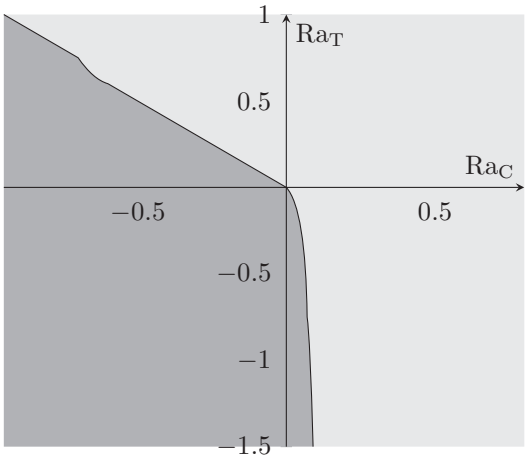

FIG. 3. Rayleigh number configurations for stable and unstable flat fronts. The values in the dark region correspond to stable flat fronts, while the ones in the light region lead to instabilities.

in stable and unstable fronts. When both Rayleigh numbers are negative there is only stable flat fronts since fluid of lower density is placed above a fluid of higher density. Having both Rayleigh numbers positive there is always a perturbation of wave number close to zero that has a positive growth rate; thus unbounded flat fronts will always be unstable. The figure also shows that when the Rayleigh numbers have opposite sign, there is a curve that separates stable from unstable domains. This curve is steeper for negative thermal Rayleigh numbers $\mathrm{Ra_T}$, indicating that a small positive $\mathrm{Ra_T}$ can lead to an instability.

B. Nonlinear system results

We study the propagation of reaction fronts with convection solving numerically the nonlinear system of equations (8). In this work we focus on thermal density changes while varying the domain width; thus the Rayleigh numbers are set to $\mathrm{Ra_T} = 0$ and $\mathrm{Ra_T} = 3$. According to the dispersion relation Fig. 1 flat fronts are stable for perturbations of large wave number (small wavelength); consequently flat fronts in narrow tubes will be stable. Perturbations with the wave number greater than $q = 2.5$ will decay exponentially (Fig. 1); thus convectionless flat fronts will propagate in rectangular domains of width less than $\mathrm{L} = \pi/q = 1.26$. For larger widths, the perturbations grow leading to the formation of fronts of steady shape and higher speed.

We obtain axisymmetric and nonaxisymmetric fronts of steady shape as the flat front loses stability in wider domains. Here the axis is defined as a line pointing in the vertical y direction, halfway between the walls. We show in Fig. 4(a) the shape of the front and the fluid velocity field of the nonaxisymmetric front as it propagates in a domain of width $\mathrm{L} = 5$. The front is represented with a line that separates reacted from unreacted fluid, the velocity field shows a single convective roll that lifts the front on one side of the domain, and lowers it in the opposite side. For a domain width $\mathrm{L} = 12$, the front takes a constant axisymmetric shape as it moves upward, with two counter-rotating convective rolls lifting the front at the center of the domain [Fig. 4(b)]. In these figures, the nonaxisymmetric front propagates upward with a speed of 1.39, while the axisymmetric front moves with 1.47 as measured in the laboratory frame of reference. These values are significantly higher than the flat front speed which corresponds to one in dimensionless units. Near the center of the axisymmetric front the fluid pushes the front upward, while the curvature in the eikonal relation provides a smaller normal velocity. The opposing effects of fluid flow and curvature result in a front of constant shape, traveling with constant velocity.

We calculate the temperature profile and the stream function of reaction fronts propagating with constant curvatures. In Fig. 5(a) the stream function associated with a nonaxisymmetric front exhibits a single convective roll. In this case the stream function has a local maximum near the center of the tube, corresponding to the fluid rotating clockwise. This type of fluid motion leads to a front raised higher on the left wall similar to the flow shown in Fig. 4(a). The temperature profile [Fig. 5(b)] follows the shape of the front; however, the temperature gradients across the front are not uniform. We observe hot spots developing a higher temperature near

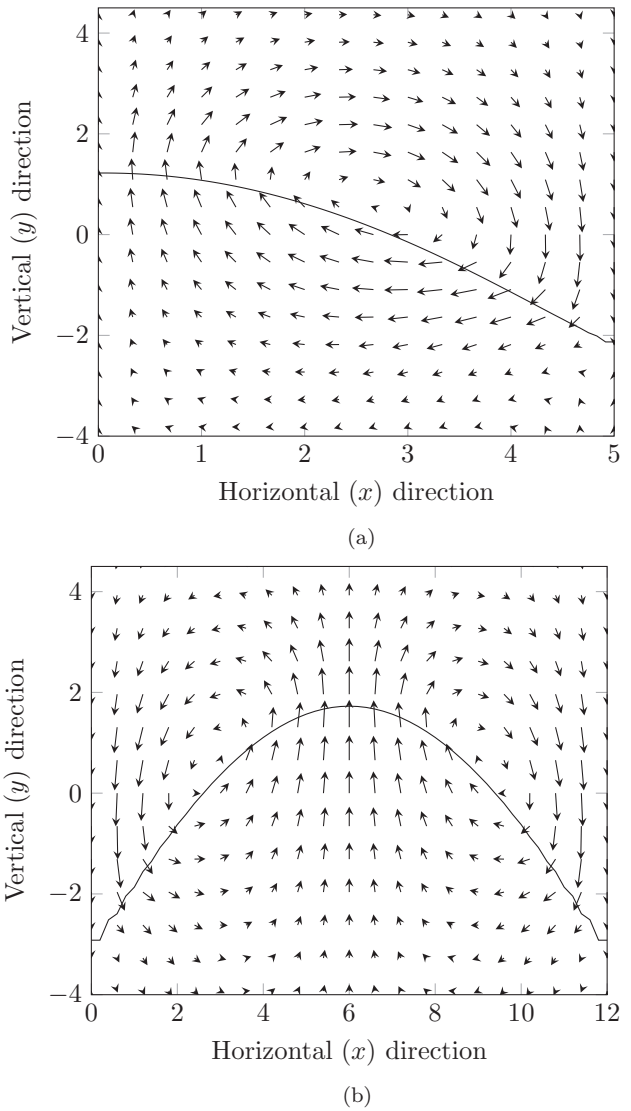

FIG. 4. Nonaxisymmetric (a) and axisymmetric (b) fronts of constant shape with corresponding velocity fields. The fronts propagate upward with constant speed. The tube widths are $\mathrm{L} = 5$ (a) and $\mathrm{L} = 12$ (b).

the wall where the front is nearly horizontal. Far behind the front, the substance is away from the heat source showing a uniform temperature that is higher that the temperature of the unreacted fluid. This is due to the heat release by the front and the insulating boundary conditions. We display in Fig. 6(a) the stream function corresponding to an axisymmetric front developed in a tube of width $\mathrm{L} = 12$. The stream function has a relative maximum and a relative minimum resulting in two counter-rotating convective rolls. In this case, the stream function is antisymmetric with respect to a reflection about the axis; thus fluid rotates in opposite directions around two rolls. The combined effect of both rolls results in having fluid rising on the center of the tube and falling near the walls. The temperature profile for the axisymmetric front shows a hot spot at the center of the tube with two other hot spots near the walls [Fig. 6(b)]. This situation is similar to the case of nonaxisymmetric fronts where hot spots appear where the

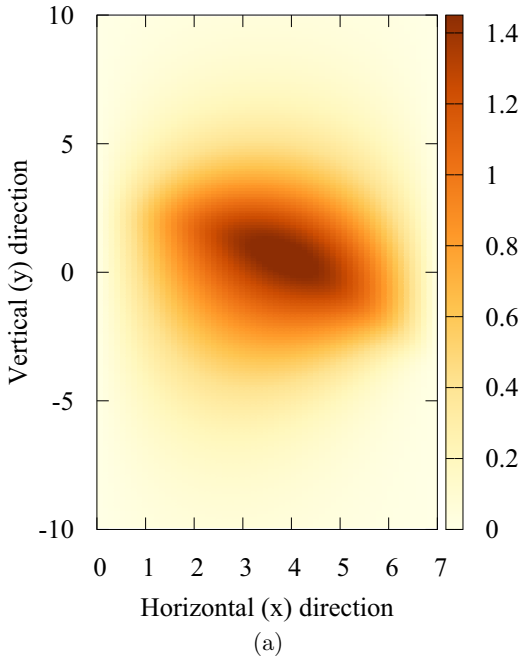

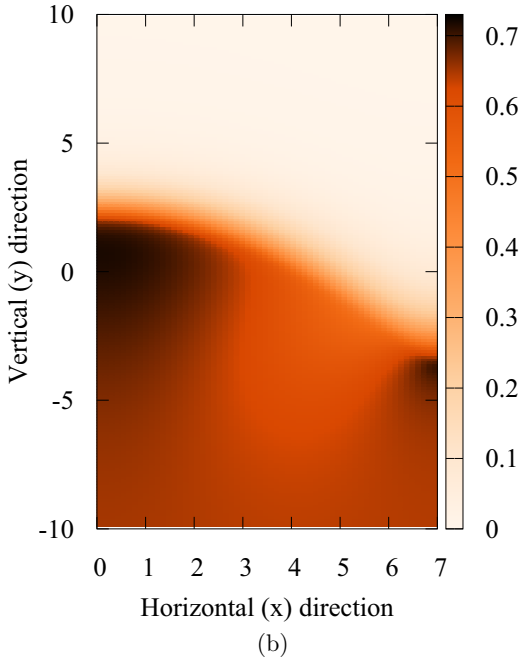

FIG. 5. Stream function (a) and temperature (b) around a nonaxisymmetric front of constant shape in a tube of width L = 6.

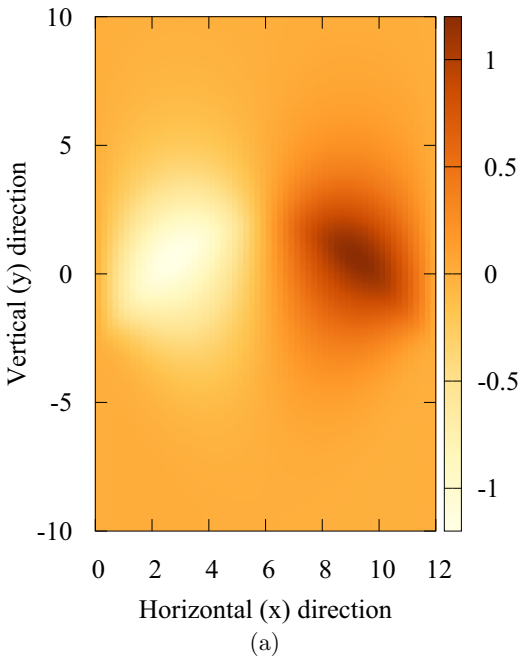

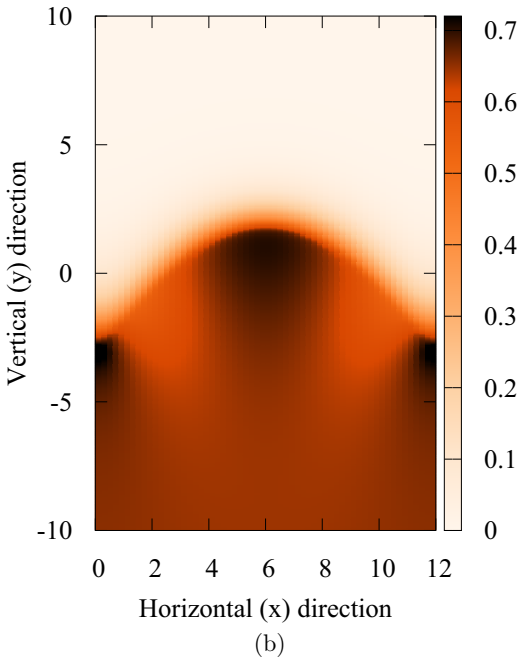

FIG. 6. Stream function (a) and temperature (b) around an axisymmetric front of constant shape in a tube of width L = 13.

slope of the front is horizontal. Hot spots have been observed in fronts propagating in the chlorite-tetrathionate reaction that are located near the trailing portions of the reaction fronts [28]. Numerical simulations of a reaction-diffusion-convection equation accounted for their location [29]. However, there are several aspects that make both systems different. Here we consider insulated boundaries while in experiments heat losses are noticed. In our confined geometry we find hot spots near the boundary walls, while experiments are carried out in a more extended Hele-Shaw cell. Although the direction of propagation of the front is different, we also find hot spots in the direction of rising fluid. We observe uniform temperatures far away from the front, with a higher temperature behind the front. As we shall see later, the uniform temperatures behind the fronts are different due to their different propagating speeds.

Figure 7(a) shows the speeds of axisymmetric and nonaxisymmetric fronts as functions of tube width. The speed of convective fronts increases in wider tubes. Convective fronts develop when the convectionless flat front loses stability; the linear stability analysis provides a critical width equal to 1.25 for these conditions. Our nonlinear results are in agreement, showing an increase of speed due to convection for tubes of width larger than the critical width. For tubes of width

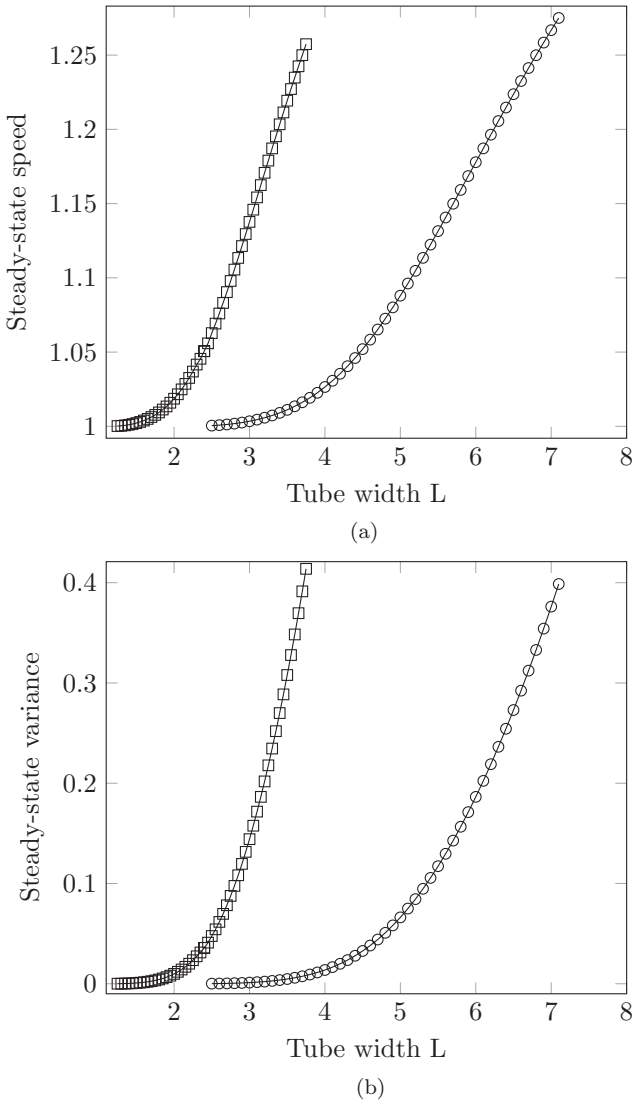

FIG. 7. Front speed (a) and variance (b) for different values of the tube width L. The curve with squares correspond to nonaxisymmetric fronts, while the circles represent axisymmetric fronts.

larger than twice the critical width, we obtain axisymmetric fronts. Although we found axisymmetric fronts from random conditions at large widths (L = 12), we could not find them close to the transition point. The results shown here correspond to axisymmetric solutions obtained by imposing the axial symmetry on the equations. Therefore, the initial axisymmetric fronts with slow speed may be unstable. The stability analysis of these fronts is beyond the scope of the present work. We point out that the axisymmetric solutions correspond to two identical nonaxisymmetric fronts mirroring one another across the axis. Therefore, the speed of an axisymmetric front corresponds to the speed of a nonaxisymmetric front in a domain half as wide. The fronts continue to deviate from the flat front as the width of the tube increases, as shown in Fig. 7(b). Here we plot the variance of the front as a function of tube width, showing that the fronts become more spread out with increasing convection.

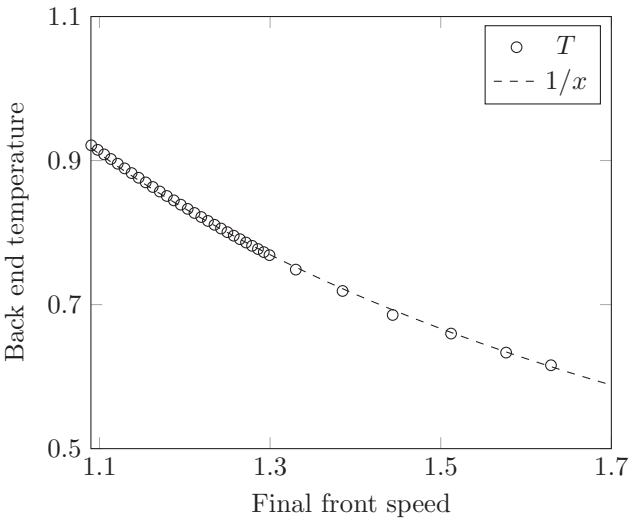

FIG. 8. Fluid temperature far behind convective fronts as a function of speed. Faster fronts correspond to a smaller increase in temperature. This temperature difference approximates an inverse relation to the speed. This result is similar to the temperature change due to a pointlike source moving with constant speed.

The temperature behind the front reaches a constant value that decreases with increasing front speed. In the case of a convectionless front, the rise in temperature is inversely proportional to the speed of the front as shown in Eq. (7). In dimensionless units flat fronts have a speed equal to one with a temperature increment equal to one. When convection takes place the speed of the front increases, lowering the temperature increment behind the front. The change in temperature for the convective front depends on the speed of the front as shown in Fig. 8. We notice that the temperature change is very close to being inversely proportional to the final speed of the convective front, as it was the case of convectionless fronts.

V. SUMMARY AND DISCUSSION

We have introduced a set of nonlinear equations describing the evolution of an exothermic reaction front in a fluid. Our model takes into account density changes due to thermal and compositional gradients which may result in convective fluid motion. For density gradients due only to thermal effects, a linear stability analysis on the flat front solutions showed that long wavelength perturbations will destabilize the front when the less dense fluid is underneath a more dense fluid, but perturbations of short wavelength will decrease in time. In this case, the critical wavelength that separates growing from decaying perturbations depends on the value of the thermal Rayleigh number. This result is also found for density changes due only to chemical composition [30]. When compositional and thermal effects are in the opposite direction the Rayleigh numbers have opposite sign. In this case the front can be unstable to perturbations in a range of wave numbers without being unstable to large perturbations.

The nonlinear equations exhibit solutions of fronts of constant shape moving steadily in narrow rectangular domains. Flat fronts in bounded domains can propagate steadily in regions of sufficiently small width. However, for widths

larger than a critical value, they lose stability becoming nonaxisymmetric fronts of higher speed. For widths larger than twice the critical width for the onset of convection, we find axisymmetric solutions that consist of two nonaxisymmetric fronts placed next to each other. Axisymmetric solutions can be found from random perturbations to the flat front only away from the onset of convection. Future work should establish the stability of both types of steady fronts.

An exothermic front moving through the fluid increases its temperature. The temperature profile exhibits regions of higher temperatures near the front; however, far behind the front the temperature is uniform, decreasing for faster moving fronts. Since convection increases the speed of the front, we also find this effect in fronts with convection. The result is similar to the one caused by a one-dimensional front, where the increase of temperature is inversely proportional to the front speed. Measurements of the temperature behind the front and the dependence with the front speed will require treatment of the heat losses, which will lower the temperature behind the front. The temperature dependence with front speed can be measured in experiments varying the width of a Hele-Shaw cell or the diameter of a tube.

ACKNOWLEDGMENT

The authors are grateful for Dirección de Gestión de la Investigación from the Pontificia Universidad Católica del Perú's funding through Grant No. 2016-3-0025.

[1] D. H. Sharp, Physica D **12**, 3 (1984).
[2] S. Chandrasekhar, *Hydrodynamic and Hydromagnetic Stability* (Oxford University Press, Oxford, 1961).
[3] G. I. Sivashinsky, Annu. Rev. Fluid Mech. **15**, 179 (1983).
[4] J. A. Pojman, R. Craven, A. Khan, and W. West, J. Phys. Chem. **96**, 7466 (1992).
[5] J. A. Pojman, I. P. Nagy, and I. R. Epstein, J. Phys. Chem. **95**, 1306 (1991).
[6] J. A. Pojman, A. Komlósi, and I. P. Nagy, J. Phys. Chem. **100**, 16209 (1996).
[7] D. Horváth, T. Bánsági, and A. Tóth, J. Phys. Chem. **117**, 4399 (2002).
[8] T. Tóth, D. Horváth, and A. Tóth, Chem. Phys. Lett. **442**, 289 (2007).
[9] G. Schuszter, G. Pótári, D. Horváth, and A. Tóth, Chaos **25**, 064501 (2015).
[10] L. Šebestíková and M. J. B. Hauser, Phys. Rev. E **85**, 036303 (2012).
[11] D. A. Vasquez, J. M. Littley, J. W. Wilder, and B. F. Edwards, Phys. Rev. E **50**, 280 (1994).
[12] A. De Wit, Phys. Rev. Lett. **87**, 054502 (2001).
[13] J. D'Hernoncourt, S. Kalliadasis, and A. De Wit, J. Chem. Phys. **123**, 234503 (2005).
[14] T. Bánsági, D. Horváth, A. Tóth, J. Yang, S. Kalliadasis, and A. De Wit, Phys. Rev. E **68**, 055301 (2003).
[15] S. Kalliadasis, J. Yang, and A. De Wit, Phys. Fluids **16**, 1395 (2004).
[16] E. Pópity-Tóth, D. Horváth, and A. Tóth, Chaos **22**, 037105 (2012).
[17] D. A. Vasquez, J. W. Wilder, and B. F. Edwards, J. Chem. Phys. **98**, 2138 (1993).
[18] J. Masere, D. A. Vasquez, B. F. Edwards, J. W. Wilder, and K. Showalter, J. Phys. Chem. **98**, 6505 (1994).
[19] J. W. Wilder, D. A. Vasquez, and B. F. Edwards, Phys. Rev. E **56**, 3016 (1997).
[20] J. W. Wilder, B. F. Edwards, and D. A. Vasquez, Phys. Rev. A **45**, 2320 (1992).
[21] E. A. Spiegel and G. Veronis, Astrophys. J. **131**, 442 (1960).
[22] J. W. Wilder, B. F. Edwards, D. A. Vasquez, and G. I. Sivashinsky, Physica D **73**, 217 (1994).
[23] B. F. Edwards, J. W. Wilder, and K. Showalter, Phys. Rev. A **43**, 749 (1991).
[24] S. E. Koonin and D. C. Meredith, *Computational Physics: Fortran Version*, The Advanced Book Program (Addison-Wesley, Redwood City, CA, 1994).
[25] W. H. Press, S. A. Teukolsky, W. T. Vetterling, and B. P. Flannery, *Numerical Recipes in Fortran 77: The Art of Scientific Computing. Volume 1 of Fortran Numerical Recipes* (Cambridge University Press, Cambridge, UK, 1997).
[26] P. N. Swarztrauber and R. A. Sweet, ACM Trans. Math. Softw. **5**, 352 (1979).
[27] D. J. Griffiths, J. Phys. A: Math. Gen. **26**, 2265 (1993).
[28] P. Grosfils, F. Dubois, C. Yourassowsky, and A. De Wit, Phys. Rev. E **79**, 017301 (2009).
[29] T. Gerard, T. Tóth, P. Grosfils, D. Horváth, A. De Wit, and A. Tóth, Phys. Rev. E **86**, 016322 (2012).
[30] D. A. Vasquez, J. W. Wilder, and B. F. Edwards, J. Chem. Phys. **104**, 9926 (1996).